# Cryo-EM reconstruction of AlfA from *Bacillus subtilis* reveals the structure of a simplified actin-like filament at 3.4-Å resolution

**Andrzej Szewczak-Harris[a] and Jan Löwe[a,1]**

[a]Medical Research Council Laboratory of Molecular Biology, Cambridge CB2 0QH, United Kingdom

Edited by James A. Spudich, Stanford University School of Medicine, Stanford, CA, and approved January 16, 2018 (received for review September 18, 2017)

**Low copy-number plasmid pLS32 of *Bacillus subtilis* subsp. *natto* contains a partitioning system that ensures segregation of plasmid copies during cell division. The partitioning locus comprises actin-like protein AlfA, adaptor protein AlfB, and the centromeric sequence *parN*. Similar to the ParMRC partitioning system from *Escherichia coli* plasmid R1, AlfA filaments form actin-like double helical filaments that arrange into an antiparallel bipolar spindle, which attaches its growing ends to sister plasmids through interactions with AlfB and *parN*. Because, compared with ParM and other actin-like proteins, AlfA is highly diverged in sequence, we determined the atomic structure of nonbundling AlfA filaments to 3.4-Å resolution by cryo-EM. The structure reveals how the deletion of subdomain IIB of the canonical actin fold has been accommodated by unique longitudinal and lateral contacts, while still enabling formation of left-handed, double helical, polar and staggered filaments that are architecturally similar to ParM. Through cryo-EM reconstruction of bundling AlfA filaments, we obtained a pseudoatomic model of AlfA doublets: the assembly of two filaments. The filaments are antiparallel, as required by the segregation mechanism, and exactly antiphasic with near eightfold helical symmetry, to enable efficient doublet formation. The structure of AlfA filaments and doublets shows, in atomic detail, how deletion of an entire domain of the actin fold is compensated by changes to all interfaces so that the required properties of polymerization, nucleotide hydrolysis, and antiparallel doublet formation are retained to fulfill the system's biological raison d'être.**

bacterial cytoskeleton | plasmid segregation | cryo-EM | helical reconstruction | actin

Actin-like proteins are defined by structural and functional homology to actin, the archetypal member of the family and the basic building block of the eukaryotic cytoskeleton (1–3). Actin-like proteins make up a functionally diverse and near-ubiquitous family of proteins. Their unifying feature is the ability to form filaments in vitro and in vivo (4, 5). All studied actin-like proteins bind and catalyze the hydrolysis of nucleotide triphosphates (especially ATP), processes that, respectively, promote filament growth and disassembly (6). Sequence database searches and structural studies revealed the presence of numerous actin homologs in bacteria and archaea, establishing the notion of the prokaryotic origin of actin-like cytoskeletal proteins (7, 8). The roles that actins fulfill in cells reflect their ability to polymerize and are especially diverse in prokaryotes, where they function in cytokinesis, morphogenesis, and DNA replication. Among the chromosomally encoded bacterial and archaeal actin-like proteins, we find: FtsA, an element of the cytokinetic (Z-) ring (9, 10); MreB, a membrane-binding protein involved in cell shape maintenance (11–13); and MamK, which organizes the distribution of magnetosomes, iron-containing organelles found in magnetotactic bacteria (14, 15). Within the archaeal phylum Crenarcheota, actin-like protein crenactin has been identified (16) as the closest so far in filament architecture and protomer (subunit) fold to eukaryotic actin (17). In addition to the housekeeping roles described above, a separate functional group evolved in the actin-like family to aid the replication of certain low copy-number plasmids, where actin-like filaments enable efficient segregation of plasmid DNA.

As plasmid DNA is replicated separately from chromosomal DNA, mechanisms that ensure the carryover of genomic material to the progeny cells do not apply to plasmids. This issue has more serious consequences for low copy-number plasmids. To address it, some of them evolved mechanisms that employ filamentous proteins to physically separate two plasmid copies and move them across cells (18). The best-studied example involves ParM, an actin-like protein, encoded by the *parMRC* locus of the R1 plasmid in Gram-negative *Escherichia coli*. The locus codes for the ParMRC system that, besides ParM, contains the DNA-binding protein ParR, and a centromeric sequence *parC* (19, 20). Principles governing plasmid segregation by the ParMRC system are well understood mechanistically. Atomic structures of the ParM filament and protomer in various nucleotide states (21, 22), as well as with ParR peptide (23), and ParR bound to *parC* (24), have been solved by X-ray crystallography and electron cryo-microscopy (cryo-EM). Reconstitution assays and total internal reflection microscopy have complemented these studies to reveal the dynamics of the filament assembly and DNA segregation (23). According to the current model, ParR binds to the *parC* sequence and acts as a seed for polymerization of ParM filaments after replication of the *parC* regions. Two filaments, each attached to a sister copy of the plasmid DNA, bundle in antiparallel pairs and grow through addition of subunits at the tips, pushing the plasmids apart (21). Conceptually, the ParMRC system is a truly minimalistic mitotic spindle apparatus.

## Significance

**Protein filaments perform a vast array of functions inside almost all living cells. Actin-like proteins in archaea and bacteria have previously been found to form a surprising diversity of filament architectures, reflecting their divergent cellular roles. Actin-like AlfA is unique in that it is much smaller than all other filament forming actin-like proteins. With an atomic structure of the AlfA filament, obtained by high-resolution electron cryo-microscopy, we have revealed—at near-atomic level of detail—how AlfA filaments form dynamic filaments capable of transporting plasmid DNA in cells and how these filaments arrange into antiparallel bundles required for the segregation mechanism.**

Author contributions: A.S.-H. and J.L. designed research, performed research, analyzed data, and wrote the paper.

The authors declare no conflict of interest.

This article is a PNAS Direct Submission.



Data deposition: The atomic coordinates have been deposited in the Protein Data Bank, www.wwpdb.org (PDB ID code 6F95) and the map deposition in the EMDataBank (EMDB ID code: EMD-4196).

See Commentary on page 3205.

[1]To whom correspondence should be addressed. Email: jyl@mrc-lmb.cam.ac.uk.

This article contains supporting information online at www.pnas.org/lookup/suppl/doi:10.1073/pnas.1716424115/-/DCSupplemental.

Published online February 13, 2018.

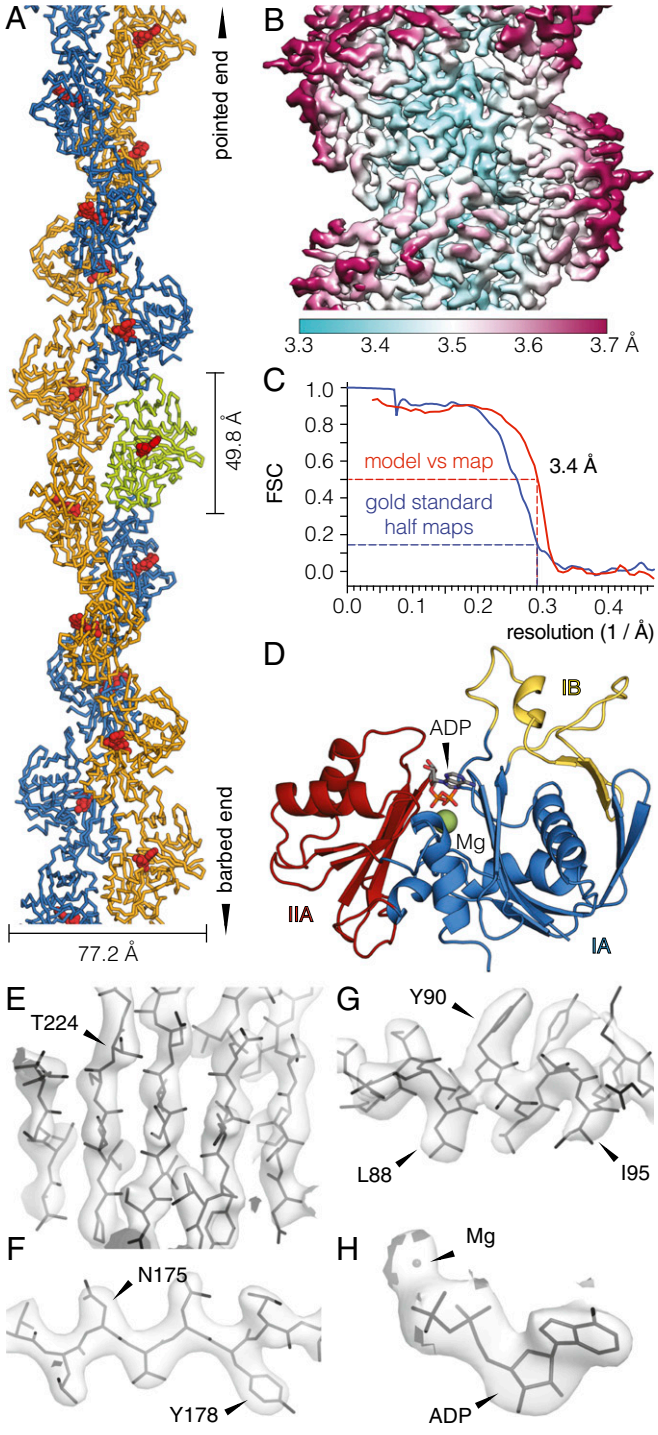


**Fig. 1.** Cryo-EM reconstruction of AlfA filament. (*A*) Refined atomic model of AlfA filament. The subunits are staggered in a left-handed, double-helical, parallel (polar) filament, with a rise of 24.9 Å and a 156.5° twist. The two protofilaments are colored orange and blue, and the bound nucleotide is red. A single AlfA protomer is highlighted in green. See also Movie S2, indicating the five built and refined subunits in two protofilaments. (*B*) Central portion of the cryo-EM density used to build the atomic model of AlfA, colored by local resolution. (*C*) Gold-standard FSC curves as calculated in RELION (32), showing the correlation between the half-datasets (blue line) and between the map and the model (red line). The overall resolution is 3.4 Å, as judged by the $FSC_{0.143}$ and $FSC_{0.5}$ criteria (blue and red dashed lines). (*D*) Atomic model of AlfA protomer, in cartoon representation, built from and refined against the cryo-EM density. Highlighted are subdomains IB, IA and IIA of the actin fold (yellow, blue and red, respectively), as well as the ADP nucleotide. (*E*–*H*) Selected portions of the cryo-EM density, showing the reconstructed map around representative secondary structural features: β-sheet (*E*), strand (*F*), and α-helix (*G*), as well as nucleotide density with coordinated magnesium (*H*). Arrowheads point to selected amino acid residues. See also Movie S1.

A similar system was identified in a strain of Gram-positive bacterium *Bacillus subtilis*, subsp. *natto*, used in the fermentation of Japanese food *nattō* from soya bean (*Glycine max*). There, a cryptic, low copy-number plasmid, pLS32, was found to contain a region responsible for conferring plasmid stability (25–27). Analogous to ParMRC, the plasmid-maintenance system of pLS32 contains an actin-like protein AlfA (28), a DNA-binding adaptor AlfB of unknown structure, and a centromeric sequence *parN* (29). Although the details of filament dynamics differ between AlfA and ParM, the basic principles of plasmid segregation are preserved: AlfA filaments, bound to the *parN* sequence via the adaptor AlfB, bundle together to form antiparallel and bipolar spindles that move DNA apart (30, 31). From a structural perspective, the system remains less well characterized than ParMRC, as atomic details of the AlfA and AlfB proteins have not yet been elucidated. As indicated by sequence alignments, 31-kDa AlfA (275 aa) is so far the smallest of the identified actin-like proteins. Its reduced size is a consequence of the deletion of one of the four subdomains (IIB) present in all other members of the family. If confirmed by an atomic structural model, the deletion poses interesting questions regarding the maintenance of filament functionality. To study how the effects of the deletion are mitigated by structural adaptations in the protomer, we chose to reconstruct the atomic structure of AlfA filament using cryo-EM.

## Results and Discussion

**Cryo-EM Reconstruction of AlfA Shows Double-Helical, Parallel, Left-Handed Filaments at Near-Atomic Resolution.** A previous study established that AlfA polymerized in the presence of ATP to form doublets of protofilaments (strands) that wrap around each other in a left-handed helix (30). The analysis was carried out with conventional, room-temperature EM using negatively stained samples, which limited the resolution to around 15 Å. To obtain a detailed, near-atomic model of the filament structure, we turned to cryo-EM, which has recently shown great success in providing such information for actin, ParM, MamK, and crenactin filaments (2, 14, 17, 21).

We began our study of the AlfA filament structure with the wild-type protein derived from the pLS32 plasmid and produced in *E. coli*. Purified protein was polymerized via the addition of ATP, deposited on a cryo-EM sample grid, vitrified, and imaged in an electron microscope (Fig. S1*A*). Similar to previously published negative-stain images of native AlfA (30), we observed heavy bundling of the filaments, alleviated only by raising the salt (KCl) concentration to 1,000 mM (Fig. S1 *B*–*D*). Disruption of bundles and obtaining single AlfA filaments is necessary for filament reconstruction; however, increasing the salt concentration significantly decreases contrast of the cryo-EM images (Fig. S1 *B*–*D*). This leads to a decrease in signal-to-noise ratio, preventing high-resolution structure determination. To obtain single filaments of AlfA, we turned to a nonbundling protein variant, described previously (30). The nonbundling AlfA is a quadruple mutant (K21A, K22A, K101A, K102A) designed to abolish the electrostatic interactions between residues implicated, through structural modeling, in bundle formation. Cryo-EM imaging of a polymerized nonbundling AlfA mutant confirmed the presence of single filaments in a low-salt background, suitable for further processing (Fig. S1*E*).

AlfA structure solution was carried out by exploiting the helical reconstruction capabilities implemented in RELION (32). The method involves single particle-like processing of helical assemblies in a Bayesian, empirical framework, using a marginalized likelihood function and priors (including a reference

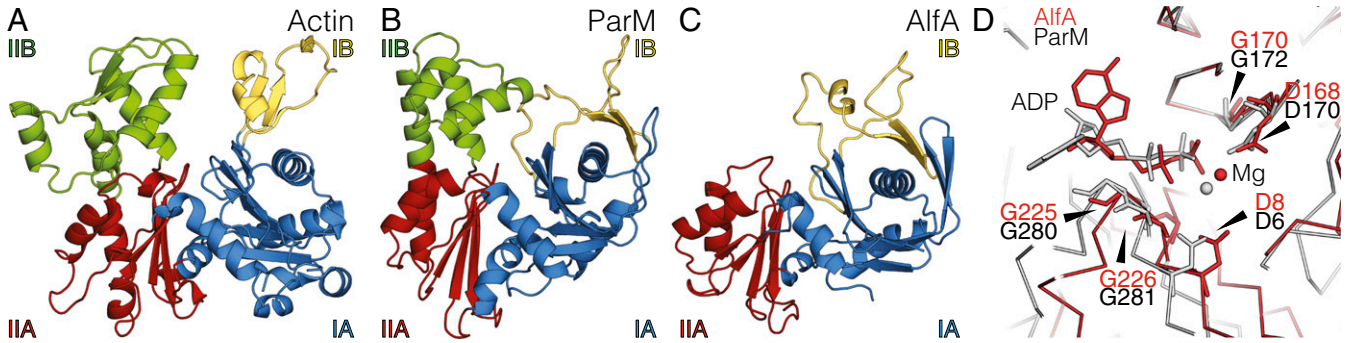


**Fig. 2.** Structural features of AlfA protomer. (*A*–*C*) Differences in fold and subdomain composition of three actin-like proteins: (*A*) F-actin from *Oryctolagus cuniculus*, (*B*) ParM from *E. coli* plasmid R, and (*C*) AlfA from *B. subtilis* plasmid pLS32 (present study). Structural domains of proteins are colored and labeled by their homology to subdomains IA (blue), IB (yellow), IIA (red), and IIB (green) (34). Deletion of the entire subdomain IIB in AlfA is evident (*C*), in agreement with amino acid sequence alignments (Fig. S3). F-actin and ParM are from PDB depositions 3J8A and 5AEY (in all figures). See also Fig. S4. (*D*) Amino acid backbone ($C_\alpha$) trace of AlfA (red) and ParM (gray) protomers in the polymerized filament, showing the ADP binding mode and the positions of conserved residues postulated to be involved in nucleotide hydrolysis. The conformation of the bound nucleotide shows the adenosine moiety rotated away from the *adenosine doublet* (G225, G226) by around 120°. In all other studied actin-like proteins, this doublet comes in contact with the adenosine; however, in AlfA, the moiety is uniquely placed between residues F12 and Y225 (Fig. S5*B*), which are not conserved in other actins (Fig. S3). Rotated adenosine is also shown in Movie S3.

model) on the reconstruction, to dampen high spatial-frequency information where there is an absence of relevant empirical data (33). Initial, reference-free 2D classification showed that individual AlfA filament segments could be effectively averaged to reveal the double-helical nature of the filament with staggered subunits, as well as secondary structure features (Fig. S1*F*). As 3D reference for the 3D refinement, we used a ParM crystal structure (PDB ID code 1MWM), which was extended in silico into a helix using parameters deduced from the 2D classes and previously published data (30). The model was low-pass–filtered to 30 Å to prevent emergence of higher-resolution structural features absent from the experimental data. The procedure involved real-space optimization of helical symmetry parameters at each of the cycles of the refinement and yielded final values of 156.5° (twist) and 24.9 Å (rise). To prevent overfitting, overlapping segments from each filament were kept in the same half-set used to calculate Fourier shell correlation (FSC).

The cryo-EM map obtained in the final step of the 3D refinement has an overall resolution of ∼3.4 Å (Fig. 1 *B* and *C*), calculated using the $FSC_{0.143}$ gold-standard criterion. As expected at this level of detail, the map clearly resolves secondary structure features as well as side-chain densities for the bulkier residues (Fig. 1 *E*–*G* and Movie S1). The density of the nucleotide bound in the catalytic pocket is clear and allowed the fitting of an ADP molecule, as well as the coordinating magnesium ion, which is also well resolved (Fig. 1*H*). Based on the density map, we built and refined a complete atomic model of a short stretch of the AlfA filament containing five protomers (Fig. 1 *A* and *D* and Movie S2). The model shows a left-handed, double-helical, parallel (polar) filament with staggered subunits, each bound to ADP, as expressed by the formula $2p(AlfA_{AXP})^N$ (34). The AlfA filament is most similar to the ParM filament in terms of its order, polarity, and handedness, but forms tighter coils, as reflected in the difference of the helical twist: 156.5° for AlfA (left turn of 47° between subunits along one AlfA protofilament) and 165.1° for ParM (left turn of 29.8° between subunits) (Fig. S2).

**The AlfA Protomer Structure Shows a Subdomain Deletion and an Unusual Nucleotide-Binding Mode.** For all previous actin-like filament structures determined by cryo-EM, reliable protomer structures obtained by X-ray crystallography were available to guide model building (6, 14, 21). With AlfA, such aid was not at hand, and all our efforts to crystallize AlfA yielded only poorly diffracting crystals. However, the cryo-EM map of AlfA was good enough for assisted de novo structure solution. The initial model, generated computationally by homology modeling, was manually fitted, adjusted, and refined to best explain the cryo-EM density. Model statistics are very good and refinement of the atomic model against the density map was performed both in

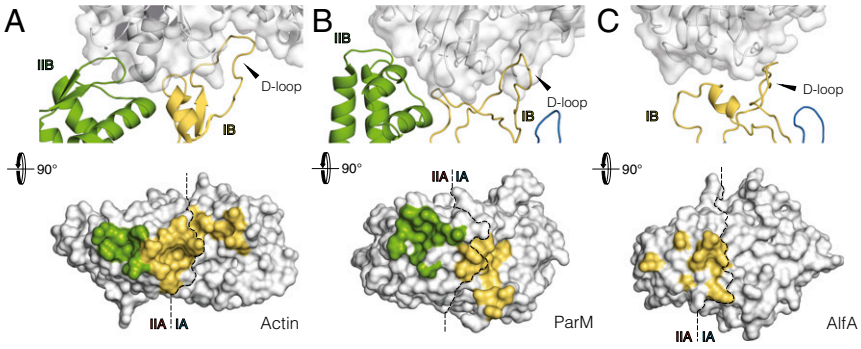


**Fig. 3.** Longitudinal interfaces of actin-like filaments. (*A*–*C*) Longitudinal (intraprotofilament/strand) interactions in F-actin (*A*), ParM (*B*), and AlfA (*C*). In each of the three examples, the D-loop of the IB subdomain of one protomer in the protofilament makes contact with the next protomer further up the protofilament. In AlfA (*C*), subdomain IIB, present in ParM (*B*), and F-actin (*A*), as well as other actin-like proteins, is absent and the longitudinal contact is solely via subdomain IB. (*A*–*C*, *Lower*) The same interaction is shown as an imprint onto the surface of a protofilament protomer, with colors representing amino acid residues in the 4-Å vicinity of the subdomains making the contact. The subdomain divisions of the protomer are indicated by dashed lines. AlfA shows a reduction in surface area and a shift of the IB subdomain interface in comparison with F-actin and ParM.

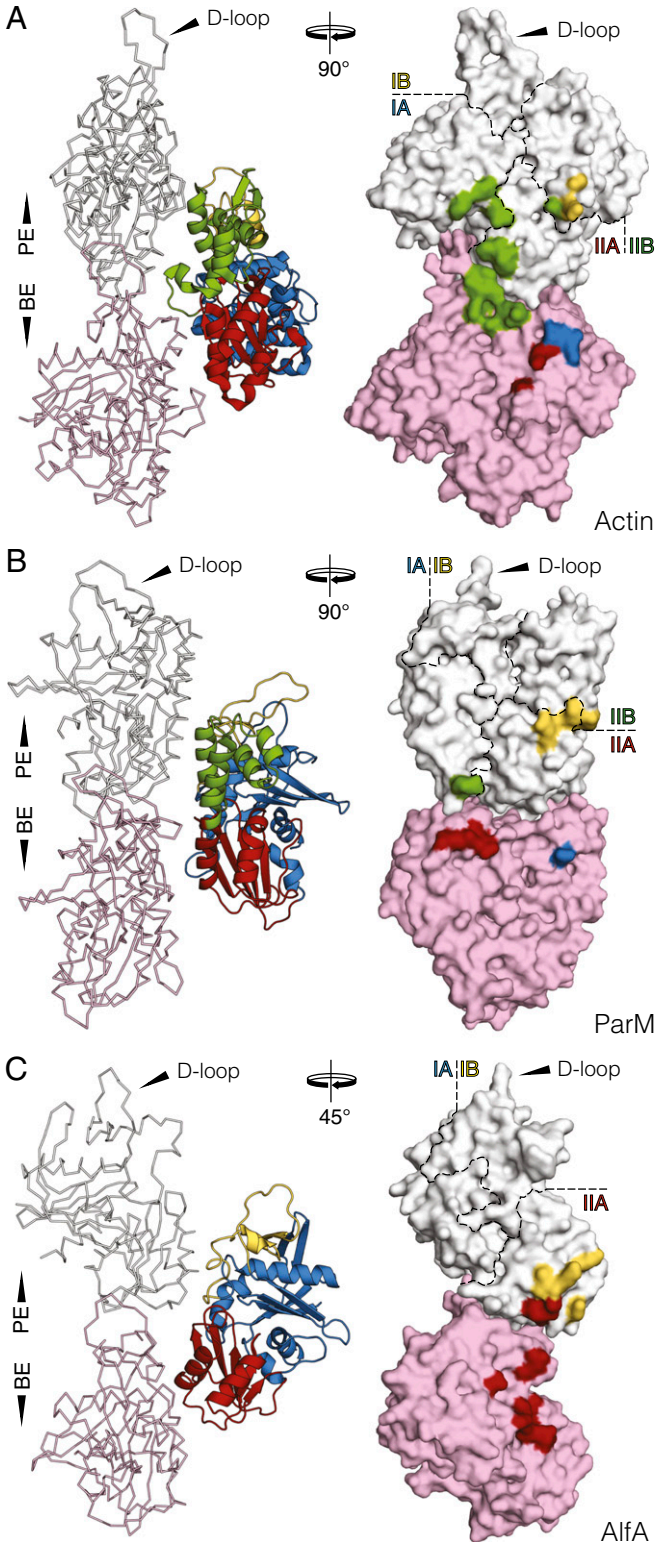


**Fig. 4.** Latitudinal interfaces of actin-like filaments. (*A*–*C*) Latitudinal (interprotofilament/strand) interactions in F-actin (*A*), ParM (*B*) and AlfA (*C*). (*Left*) For each panel, three protomers of the filament forming the latitudinal contact are shown, the axis of the filament running down the page. (*Right*) For each panel, interactions are shown as an imprint onto the surface of protofilament protomers, with colors representing amino acid residues in the 4-Å vicinity of the subdomains making the contact. As these filaments are staggered, each interacting protomer is in contact with two protomers in the opposite protofilament. The subdomain divisions of the protomer are indicated by dashed lines. Only subdomains IIA and IB of AlfA are involved in the contact, in alternating order. Abbreviations: BE, barbed end; PE, pointed end. See also Fig. S6.

real and reciprocal space, resulting in a final *R*-factor of 0.264 and a real space EMRinger score of 1.74 (Table S1).

The structure of the AlfA protomer reveals the novelty of the particular adaptation of the canonical actin fold, most notably the deletion of an entire subdomain (Fig. 2). Actins have a butterfly-like domain structure, where the nucleotide-binding pocket is found in a cleft between domains I and II (Fig. 2*A*). The domains are divided further into four subdomains: IA, IB, IIA, and IIB (or 1, 2, 3 and 4), based on the F-actin model (35). The model of AlfA obtained through our cryo-EM reconstruction clearly shows the absence of subdomain IIB, otherwise present in all other known actin-like proteins (Fig. 2 *A* and *B*). A structural alignment of representative actin-like protein sequences shows the boundaries and the position of the deletion (Fig. S3). At sequence level, AlfA is about as different from other bacterial actins ParM and MreB, as all three are from their eukaryotic counterpart (28). In the remaining subdomains, AlfA shows strongest resemblance to ParM (Fig. 2*B*), especially in how the β-hairpin from domain IB complements the β-barrel–like structure of IA to form a cradle around the central helix of this domain (perpendicular to the plane of Fig. 2*A*). When we compared the fold of AlfA to all protein structures deposited in the PDB (36), ParM occupied all top positions of the list, with the best match having a *z*-score of 9.1 and a RMSD of the amino acid backbone of 2.34 Å (Fig. S4). Considering the 18% sequence identity between ParM and AlfA, this is a striking example of conservation of structure.

AlfA was initially identified from sequences as a member of the actin-like family proteins, due to the presence of signature nucleotide-binding motifs conserved across eukaryotic actin, FtsA, MreB, and ParM (28). The motifs are found in the loops that protrude into the catalytic pocket and include: a pair called *phosphate 1* and *2*, implicated in the binding and hydrolysis of the γ-phosphate of ATP, as well as the *adenosine doublet*, vital for the positioning of the nucleotide base (1). Our sequence alignment shows all three signature sequences (Fig. S3) (37) and our structure places them in the context of the nucleotide-binding pocket of the protein (Fig. S5*A*). The *phosphate 1* motif is composed of residues D8 and G10 of AlfA and *phosphate 2* is D168 and G170. The overall arrangement of the conserved aspartate residues is similar to ParM (Fig. 2*D*) as well as other actins (8, 22, 35). Furthermore, our model shows an oxygen from the γ-carboxylic group of E151 occupying one of the coordination positions of the magnesium ion (Movie S3). This glutamate is found in a similar arrangement in MreB, MamK, and ParM and is also possibly involved in the ATP hydrolysis (14, 23, 38). The cryo-EM density strongly indicates the presence of ADP in the nucleotide-binding pocket (Fig. 1*H*), suggesting the majority of the added ATP had been hydrolyzed by AlfA before the grid was vitrified.

The catalytic nucleotide-binding pocket of AlfA, while very similar to other actins, shows one striking structural difference. The *adenosine doublet* (G225, G226), although conserved in AlfA in the usual position, does not contact the nucleotide base as expected. Instead, the adenosine moiety of ADP is swung out by about 120° from the vicinity of the doublet (Fig. 2*D* and Movie S3). In our model, the adenine purine ring of the nucleotide is instead sandwiched between a pair of aromatic residues F12 and Y255 (Fig. S5*B*), which are not conserved across the family (Fig. S3). It has been shown that AlfA accepts the other purine nucleotide GTP (30), and this can be explained by the fact that the differentially substituted positions of the purine rings (C2 and C6) are not in contact with the protein. Other actin-like proteins also have the ability to hydrolyze both nucleotides (20, 39), likely due to the same reason.

**Loss of Subdomain IIB Is Accompanied by Changes in Longitudinal and Latitudinal Contacts of the AlfA Filament.** The subdomain deletion found in AlfA poses interesting questions about the maintenance

of protofilament (strand) contacts in the polymerized filament. All studied actin-like filament structures show a pair of protofilaments in the native state (Fig. S2). With the notable exception of MreB, the protofilaments wrap around each other in a parallel double helix. For each protomer in a double helix, we can define two types of interactions: latitudinal (interprotofilament) contacts between protomers situated in the two protofilaments, and longitudinal (intraprotofilament) contacts between protomers in the same protofilament. To assess the architecture of the filament assembly and the consequences of the IIB domain deletion, we visualized the longitudinal (Fig. 3) and latitudinal (Fig. 4) contacts in our AlfA filament model. We knew from previous studies that the contacts are poorly conserved on the level of amino acid sequence between the actin-like proteins (4, 21), so we investigated the internal filament surfaces instead, taking a 4-Å radius of interaction (slightly above the upper length limit of a weak hydrogen bond).

In both actin (Fig. 3*A*) and ParM (Fig. 3*B*), the longitudinal contacts are formed through the interactions of the IIB and IB subdomains of one protomer with the IIA and IA subdomains of the other. The interaction of the IB subdomain occurs mainly via the hydrophobic D-loop, which in filamentous actin and ParM inserts into a pocket on subdomain IA (Fig. 3 *A* and *B*) in the preceding subunit of the protofilament. In AlfA, subdomain IIB is absent and so the interaction between the D-loop and the rest of the domain IB is shifted toward the IIA subdomain, with subdomain IB making no contact with the IA subdomain (Fig. 3*C*). Compared with the other protofilament structures, the remainder of the AlfA protomer in the protofilament is twisted away from its missing IIB subdomain, and the IA subdomain no longer makes any filament contacts, pushed out from the filament axis (Fig. S6). As a result, in AlfA filaments, the longitudinal contacts in the filament involve only two domains, IIA and IB, in alternating succession. Actin, ParM, and AlfA form staggered filaments, which means that each protomer interacts with two protomers on the opposite protofilament, forming latitudinal contacts that hold the double filaments together. In actin and ParM, all four subdomains make latitudinal contacts with adjacent protofilament protomers (Fig. 4 *A* and *B*). Notably, the latitudinal contacts of ParM constitute a smaller surface than those of actin and are formed by salt bridges (21). The structure of AlfA shows a more pronounced departure from the actin filament structure (Fig. 4*C*).

We undertook a quantitative analysis of the protofilament interface differences between the three analyzed examples (Table S2) (40). In actin, the longitudinal interactions cover 2,299 Å$^2$ of the molecule surface. For ParM and AlfA these values are, respectively, 1,989 and 1,051 Å$^2$, reflecting the decrease in the interaction surface shown in Fig. 3. Similarly, in the latitudinal contact, 935 Å$^2$ of each actin protomer interacts with the two protomers of the opposite protofilament. The corresponding values for ParM and AlfA are 746 and 808 Å. The increase in latitudinal contact in AlfA compared with ParM is slight; but when we look at the fraction of the total interface of AlfA involved in making the contact, it seems that the loss of subdomain IIB in AlfA places greater emphasis on the latitudinal contacts. This is perhaps not unexpected. On the whole, AlfA seems to present a further evolutionary departure from eukaryotic actin filament than ParM, not only in terms of sequence and length, but also the surface implicated in interface formation. This observation is the basis for our notion that AlfA is a simplified actin-like system: despite reductions in size and interaction surfaces, the protein still polymerizes into dynamic filaments that bind adaptors and perform mechanical, cytomotive work to fulfill their cellular function.

**Reconstruction of AlfA Doublets Show Antiparallel Arrangement Necessary for Plasmid Segregation with a Bipolar Spindle.** Previously published studies (30, 31) indicated that polymerized AlfA forms antiparallel bundles. This property is crucial for the creation of bipolar segregating spindles, as seen in the other DNA-segregating protein ParM (21). The antiparallel orientation of the filaments is necessary to ensure that when new protomers are added to the spindle, it grows in opposite directions and pushes the plasmid copies apart (23). To study the architecture of the AlfA bundles at a greater level of detail, we opted for cryo-EM to reconstruct the structure of filament arrangements formed by AlfA.

Taking our cryo-EM micrographs of polymerized, wild-type AlfA (Fig. S1 *A*–*D*), we obtained reference-free, averaged images of pairs of AlfA filaments present in the vitrified sample (Fig. 5*A*). The images clearly show the two filaments perfectly out of phase, with narrow and thin parts interlocking, as well as some secondary structural features, indicating the quality of the averaging. A close inspection of the images shows the presence of multiple twofold axes perpendicular to the plane of the doublet, suggesting that the filaments are antiparallel (rotated by 180°) (Fig. 5*A*). To determine the angular orientations of the two filaments, we projected and rotated our high-resolution AlfA model to match the averages (Fig. 5*B*). The analysis revealed that the two filaments, although running in opposite directions, have the same orientation, or in other words, are rotated around their main axes to the same angle. This observation suggests a screw-like and exactly antiphasic arrangement of the filaments in the spindle, very similar to ParM (21). Using the particles from the 2D classification, we reconstructed a 3D model of the doublet, with the single-particle mode of RELION. Resolution of the reconstruction was limited to above 10 Å, most likely due to the scarcity of side views of filament doublets in the

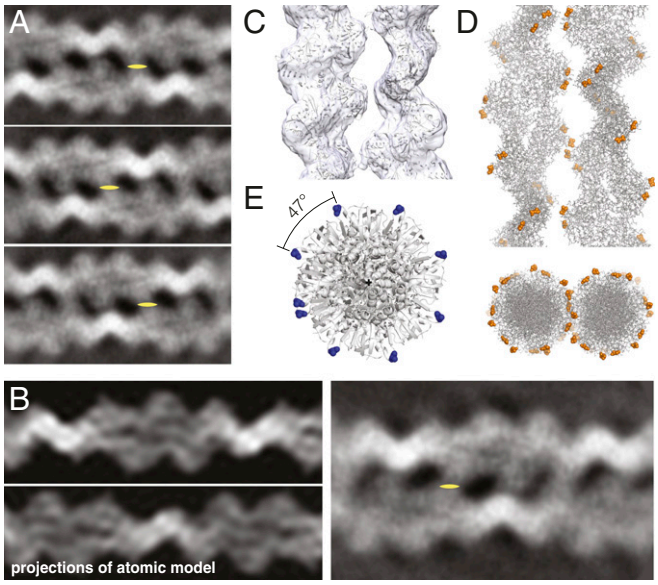


**Fig. 5.** Low-resolution cryo-EM reconstruction of AlfA filament doublet. (*A*) Representative reference-free 2D class averages of wild-type AlfA show pairs of filaments. The images show two filaments running antiparallel to each other and perfectly out of phase with the narrow part of one filament lining up with the wide part of the other. Yellow symbols indicate the positions of one of the multiple twofold symmetry axes perpendicular to the filament axis. (*B*, *Right*) Another reference-free 2D class similar to those in *A*. (*Left*) Two simulated projections of the high-resolution filament structure, rotated along the filament axis and, in the case of the *Lower* projection, flipped into antiparallel orientation, so that both match the experimental 2D class average on the *Right*. (*C*) Cryo-EM envelope of the AlfA filament doublet, reconstructed from 2D-classified segments using single-particle, nonhelical mode of RELION. Two filaments have been fitted into the obtained density and the resulting orientations match the orientations derived from the projection matching in *B*. (*D*, *Upper*) Side and top view (*Lower*) of the doublet model, in stick representation, with orange spheres indicating the positions of the lysine residues K21, K22, K101, and K102 that reduce bundling upon mutation to alanine. (*E*) A look down the filament axis with A22 marked in blue, showing the almost perfect eightfold symmetry of the filament (47° between subunits in one protofilament). We propose that the close to eightfold symmetry enables efficient bundling into doublets.

micrographs, but it allowed us to fit the AlfA filament models into the density envelope (Fig. 5*C*). The reconstruction shows the two filaments arranged in the predicted antiparallel fashion, according to angles derived from projection matching (Fig. 5*D*).

Individual protomers in each protofilament of the AlfA filament are related by a left-handed twist of 47° (Fig. 5*E*). Consequently, when viewed down the main filament axis, the subunits show an almost perfect eightfold (octagonal) symmetry (Fig. 5*E*). Thus, when two filaments associate into an antiparallel doublet, the interfilament interactions holding the filaments together are (almost) preserved in each turn of the helix by the symmetries of the filaments. The twist of the high-resolution structure model deviates from the perfect eightfold symmetry by 2°, but in principle could be adjusted for by a superhelical twist of the doublet or conformational variation; indeed, some degree of flexibility is seen in the AlfA filament (Fig. S1). Another striking example of this type of doublet symmetrization is observed in the ParM filament, where the protofilament protomer rotation of 29.8° creates an almost perfect 12-fold symmetry (21, 23).

**Implications of Plasmid Evolution on Structure of AlfA Filament.** On the level of sequence and structure, AlfA represents the furthest evolutionary detour from the canonical actin-like protein model. Despite the striking structural differences described here, AlfA still forms actin-like filaments, which in their function and construction are very close to ParM. Both proteins hydrolyze ATP, polymerize into bipolar spindles, and are capable of segregating plasmid DNA with the aid of an accessory protein and a centromeric sequence. Now we are able to show that ParM and AlfA also share a common architectural paradigm: maintenance of filament symmetry that ensures the formation of antiparallel filament pairs. For AlfA it is realized through most economical means, which involve a structural subdomain deletion accompanied by an overall reduction of total filament interface area. The reasons that caused the deletion as well as its evolutionary past are unclear. It may be that it captures particular aspects of plasmid evolution, such as a strong drive toward functional simplification and sequence reduction. In any case, AlfA is a perfect example of streamlining functionality and complexity, a distinctive manifestation of a DNA-segregation system, which is able to effectively separate 70-kbp pieces of DNA with just two proteins and some ATP.

## Materials and Methods

Details of the procedures below are given in *SI Materials and Methods*. Briefly, both AlfA constructs (wild-type and nonbundling) were expressed in *E. coli* as lipoyl domain fusions and extracted using metal affinity chromatography. The fusion protein was cleaved with tobacco etch virus (TEV) protease and further purified using size-exclusion chromatography. AlfA was polymerized at 0.5 mg/mL in 20 mM Tris·HCl, 100 mM KCl, 2 mM Tris(2-carboxyethyl)phosphine (TCEP), 1 mM $NaN_3$, pH 8.0 with 5 mM ATP and 10 mM $MgCl_2$. The sample was applied to a cryo-EM grid and vitrified in liquid ethane. For AlfA structure solution with the nonbundling mutant, the grids were imaged using Titan Krios G3 transmission electron microscope (TEM; FEI) and Falcon III EC direct electron detector (FEI). For doublet structure solution with wild-type AlfA, a Tecnai Polara G2 TEM (FEI) and Falcon III were used. Cryo-EM reconstruction of the filament was done in RELION (32), using the helical method (33). The atomic model of AlfA was built manually and refined (Table S1). For the doublet structure solution, the filaments were treated as single particles, not helical segments. The refined structure was deposited in the PDB with ID code 6F95, and the corresponding cryo-EM 3D map was deposited in the EMDataBank (EMDB) with ID code EMD-4196.

**ACKNOWLEDGMENTS.** This work was funded by the Medical Research Council Grant U105184326 (to J.L.) and Wellcome Trust Grant 095514/Z/11/Z (to J.L.).

1. Bork P, Sander C, Valencia A (1992) An ATPase domain common to prokaryotic cell cycle proteins, sugar kinases, actin, and hsp70 heat shock proteins. *Proc Natl Acad Sci USA* 89:7290–7294.
2. von der Ecken J, et al. (2015) Structure of the F-actin-tropomyosin complex. *Nature* 519:114–117.
3. Pollard TD, Shelton E, Weihing RR, Korn ED (1970) Ultrastructural characterization of F-actin isolated from *Acanthamoeba castellanii* and identification of cytoplasmic filaments as F-actin by reaction with rabbit heavy meromyosin. *J Mol Biol* 50:91–97.
4. Derman AI, et al. (2009) Phylogenetic analysis identifies many uncharacterized actin-like proteins (Alps) in bacteria: Regulated polymerization, dynamic instability and treadmilling in Alp7A. *Mol Microbiol* 73:534–552.
5. Stoddard PR, Williams TA, Garner E, Baum B (2017) Evolution of polymer formation within the actin superfamily. *Mol Biol Cell* 28:2461–2469.
6. Izoré T, van den Ent F (2017) Bacterial Actins. *Prokaryotic Cytoskeletons*, eds Löwe J, Amos LA. Subcellular Biochemistry, ed Harris JR (Springer, Cham, Switzerland), pp 245–266.
7. Cabeen MT, Jacobs-Wagner C (2010) The bacterial cytoskeleton. *Annu Rev Genet* 44: 365–392.
8. van den Ent F, Amos LA, Löwe J (2001) Prokaryotic origin of the actin cytoskeleton. *Nature* 413:39–44.
9. Pichoff S, Lutkenhaus J (2005) Tethering the Z ring to the membrane through a conserved membrane targeting sequence in FtsA. *Mol Microbiol* 55:1722–1734.
10. Szwedziak P, Wang Q, Freund SMV, Löwe J (2012) FtsA forms actin-like protofilaments. *EMBO J* 31:2249–2260.
11. Doi M, et al. (1988) Determinations of the DNA sequence of the mreB gene and of the gene products of the mre region that function in formation of the rod shape of *Escherichia coli* cells. *J Bacteriol* 170:4619–4624.
12. Jones LJ, Carballido-López R, Errington J (2001) Control of cell shape in bacteria: Helical, actin-like filaments in *Bacillus subtilis*. *Cell* 104:913–922.
13. Salje J, van den Ent F, de Boer P, Löwe J (2011) Direct membrane binding by bacterial actin MreB. *Mol Cell* 43:478–487.
14. Löwe J, He S, Scheres SHW, Savva CG (2016) X-ray and cryo-EM structures of monomeric and filamentous actin-like protein MamK reveal changes associated with polymerization. *Proc Natl Acad Sci USA* 113:13396–13401.
15. Ozyamak E, Kollman J, Agard DA, Komeili A (2013) The bacterial actin MamK: In vitro assembly behavior and filament architecture. *J Biol Chem* 288:4265–4277.
16. Ettema TJG, Lindås A-C, Bernander R (2011) An actin-based cytoskeleton in archaea. *Mol Microbiol* 80:1052–1061.
17. Izoré T, Kureisaite-Ciziene D, McLaughlin SH, Löwe J (2016) Crenactin forms actin-like double helical filaments regulated by arcadin-2. *eLife* 5:e21600.
18. Gerdes K, Howard M, Szardenings F (2010) Pushing and pulling in prokaryotic DNA segregation. *Cell* 141:927–942.
19. Jensen RB, Gerdes K (1997) Partitioning of plasmid R1. The ParM protein exhibits ATPase activity and interacts with the centromere-like ParR-parC complex. *J Mol Biol* 269:505–513.
20. Popp D, et al. (2008) Molecular structure of the ParM polymer and the mechanism leading to its nucleotide-driven dynamic instability. *EMBO J* 27:570–579.
21. Bharat TAM, Murshudov GN, Sachse C, Löwe J (2015) Structures of actin-like ParM filaments show architecture of plasmid-segregating spindles. *Nature* 523:106–110.
22. van den Ent F, Møller-Jensen J, Amos LA, Gerdes K, Löwe J (2002) F-actin-like filaments formed by plasmid segregation protein ParM. *EMBO J* 21:6935–6943.
23. Gayathri P, et al. (2012) A bipolar spindle of antiparallel ParM filaments drives bacterial plasmid segregation. *Science* 338:1334–1337.
24. Schumacher MA, et al. (2007) Segrosome structure revealed by a complex of ParR with centromere DNA. *Nature* 450:1268–1271.
25. Tanaka T, Koshikawa T (1977) Isolation and characterization of four types of plasmids from *Bacillus subtilis* (*natto*). *J Bacteriol* 131:699–701.
26. Tanaka T, Ogura M (1998) A novel *Bacillus natto* plasmid pLS32 capable of replication in *Bacillus subtilis*. *FEBS Lett* 422:243–246.
27. Tanaka T (2010) Functional analysis of the stability determinant AlfB of pBET131, a miniplasmid derivative of *Bacillus subtilis* (*natto*) plasmid pLS32. *J Bacteriol* 192: 1221–1230.
28. Becker E, et al. (2006) DNA segregation by the bacterial actin AlfA during *Bacillus subtilis* growth and development. *EMBO J* 25:5919–5931.
29. Tanaka T, Ishida H, Maehara T (2005) Characterization of the replication region of plasmid pLS32 from the *natto* strain of *Bacillus subtilis*. *J Bacteriol* 187:4315–4326.
30. Polka JK, Kollman JM, Agard DA, Mullins RD (2009) The structure and assembly dynamics of plasmid actin AlfA imply a novel mechanism of DNA segregation. *J Bacteriol* 191:6219–6230.
31. Polka JK, Kollman JM, Mullins RD (2014) Accessory factors promote AlfA-dependent plasmid segregation by regulating filament nucleation, disassembly, and bundling. *Proc Natl Acad Sci USA* 111:2176–2181.
32. Scheres SHW (2012) RELION: Implementation of a Bayesian approach to cryo-EM structure determination. *J Struct Biol* 180:519–530.
33. He S, Scheres SHW (2017) Helical reconstruction in RELION. *J Struct Biol* 198:163–176.
34. Ghosal D, Löwe J (2015) Collaborative protein filaments. *EMBO J* 34:2312–2320.
35. Kabsch W, Holmes KC (1995) The actin fold. *FASEB J* 9:167–174.
36. Krissinel E, Henrick K (2004) Secondary-structure matching (SSM), a new tool for fast protein structure alignment in three dimensions. *Acta Crystallogr D Biol Crystallogr* 60:2256–2268.
37. Pei J, Kim B-H, Grishin NV (2008) PROMALS3D: A tool for multiple protein sequence and structure alignments. *Nucleic Acids Res* 36:2295–2300.
38. van den Ent F, Izoré T, Bharat TAM, Johnson CM, Löwe J (2014) Bacterial actin MreB forms antiparallel double filaments. *eLife* 3:e02634.
39. Popp D, et al. (2010) Filament structure, organization, and dynamics in MreB sheets. *J Biol Chem* 285:15858–15865.
40. Krissinel E, Henrick K (2007) Inference of macromolecular assemblies from crystalline state. *J Mol Biol* 372:774–797.